

Short Communication

## Corrosion Behavior of Reduced-Graphene-Oxide-Modified Epoxy Coatings on N80 Steel in 10.0 wt% NaCl Solution

Chun Feng<sup>1,2,\*</sup>, Yaqiong Cao<sup>1,2,\*</sup>, Lijuan Zhu<sup>1,2,\*</sup>, Zongxue Yu<sup>3</sup>, Guhui Gao<sup>4</sup>, Yacong Song<sup>1,2</sup>, Hongjiang Ge<sup>5</sup>, Yaxu Liu<sup>1,2</sup>

<sup>1</sup> CNPC Tubular Goods Research Institute, Xi'an, Shaanxi, China, 710077.

<sup>2</sup> State Key Laboratory for Performance and Structure Safety of Petroleum Tubular Goods and Equipment Materials, Xi'an, 710077, China.

<sup>3</sup> Southwest Petroleum University, Chengdu, Sichuan, China, 6110500.

<sup>4</sup> TsinghuaRedbud Innovation Institute, Baodi, Tianjin, China, 301800.

<sup>5</sup> Oil Production Technology Research Institute of Petrochina Dagang Oilfield Company, Tianjin, China, 300280.

\*E-mail: [fengchun003@cnpc.com.cn](mailto:fengchun003@cnpc.com.cn), [caoyaqiong1992@163.com](mailto:caoyaqiong1992@163.com), [zhulijuan1986@cnpc.com.cn](mailto:zhulijuan1986@cnpc.com.cn)

Received: 30 January 2020 / Accepted: 31 March 2020 / Published: 10 July 2020

---

This study is examined the effects of modified epoxy (EP) coatings with various contents of reduced graphene oxide (RGO) in oil and gas production environments with high-temperature and high-salinity on the long-term service performance of N80 steel. The fracture surfaces of RGO-modified EP coatings were characterized by scanning electron microscopy (SEM). The corrosion resistance of the coatings after immersion in 10.0 wt% NaCl solution for 60 days at 50°C was characterized via electrochemical impedance spectroscopy (EIS) and using potentiodynamic polarization curves. After immersion in the 10.0 wt% NaCl solution for 60 days, the EP composite coatings with 1.0 wt% RGO nanosheets still showed improved strength and toughness compared with the EP coatings, with pores that were two to three times smaller and two orders of magnitude less numerous than the neat EP coatings, which resulted in excellent corrosion resistance.

---

**Keywords:** Reduced graphene oxide, epoxy, high temperature, high salinity, corrosion resistant

### 1. INTRODUCTION

Epoxy (EP) coatings have been widely used in the corrosion protection of tubing due to the excellent adhesion properties, low shrinkage, low price, and outstanding chemical stability of epoxy [1-6]. However, with the development of ultra-deep oil fields, the problem of tubing corrosion is more severe due to the high-temperature and high-salinity exploitation environment [7,8]. In onshore oilfields with high sodium chloride content of the formation brine, such as Pucheng oilfield, in which the Na<sup>+</sup>

content is  $(8.5\sim 14.5) \times 10^4$  mg/L and the  $\text{Cl}^-$  content is  $(19.15\sim 22.50) \times 10^4$  mg/L [9], the corrosion of N80 tubing is extremely severe [10,11]. In these high-temperature and high-salinity exploitation environments, limitations of EP coatings are exposed: the high degree of crosslinking density renders them brittle, thereby reducing their fracture toughness [12,13], and they exhibit poor resistance to crack propagation [1]. Defects, such as pin holes, easily occur after curing [13]. Corrosive electrolytes, such as small molecules, especially  $\text{Cl}^-$  in high-salinity and high-temperature environments, will penetrate these cracks and pores to form corrosion products under the coatings. Therefore, the EP coatings can't provide long-term corrosion protection [14,15]. Fillers are typically added to improve the corrosion resistance of EP coatings [16-21].

In recent years, graphene has attracted extensive attention due to its substantial potential in improving the properties of resin-based materials and excellent physical properties. Graphene that is well-dispersed in the voids of the coatings can improve the compactness of the coatings, and the lamellar structure of graphene can effectively prevent the permeation of corrosive media, such as  $\text{H}_2\text{O}$ ,  $\text{O}_2$  and  $\text{Cl}^-$ , thereby resulting in excellent corrosion resistance of the graphene-modified coatings [19-22]. The effects of graphene addition on the corrosion resistance of EP coatings in simulated seawater and normal atmospheric temperature environments have been widely reported [23-29]. Feng [30] prepared  $\beta$ -CD-g-GO/epoxy coatings and found that composite coatings showed satisfactory corrosion resistance after 36 hours of immersion in 3.5 wt% NaCl solution at room temperature. In reference [31], 2.0 wt% 3-aminopropyltrimethoxysilane (APTMS-GO) nanosheets were added into the EP coating, which was subsequently immersed in 3.5 wt% NaCl solution at room temperature. The results demonstrate that the coatings exhibited satisfactory corrosion resistance. However, the corrosion resistances of graphene-modified EP coatings in high-salinity and high-temperature oil production environments are seldom reported.

In our previous study [32], RGO-reinforced EP composite coatings were prepared on N80 steel. These composite coatings showed improved adhesion, toughness, and corrosion resistance after immersion in simulated oil and gas production environments with high-temperature and high-salinity at  $80^\circ\text{C}$  for 10 hours. The addition of 1.0 wt% RGO nanosheets effectively reduced the number and size of the pores in the as-prepared EP composite coatings. However, quantitative expressions and variation rules of the sizes of the pores in the EP composite coatings after corrosion testing with the contents of RGO have not been defined, and the long-term service performances of RGO reinforced EP composite coatings in oil and gas production environments remain unclear. The working temperature of most water injection tubings is approximately  $50^\circ\text{C}$ . However, the corrosion resistances of RGO-modified EP coatings in high-salinity and high-temperature oil production environments at  $50^\circ\text{C}$  for long times are rarely reported.

Therefore, the corrosion resistance of RGO-modified EP coatings that are immersed in 10.0 wt% NaCl solution for 60 days at  $50^\circ\text{C}$  was studied via EIS and potentiodynamic polarization curves in this study. In addition, the morphology and microstructure of the RGO was analyzed via FTIR and TEM. The fracture surfaces of RGO-modified EP coatings were characterized via SEM, and quantitative expressions and variation rules for the sizes of pores in the EP composite coatings as functions of the RGO content were defined.

## 2. EXPERIMENTAL

### 2.1. Preparation of modified EP coatings

N80 tubing samples (200 mm×20 mm×3 mm) are selected as coating spraying substrates. The specimens were polished with silicon carbide paper and cleaned in an ultrasonic cleaner. The cleaning solution consisted of acetone and ethanol, and the steel substrates were reserved after drying. RGO was mixed into an organic solvent (0.8 g/L), and the mixture was dispersed in an ultrasonic disperser. The prepared dispersions were added into EP coatings (solid content of 61.0 wt%) for magnetic stirring, and the stirring time was 15 min. The mixed slurries of RGO with various contents (0 wt%, 0.5 wt%, 1.0 wt%, 2.5 wt% and 4.0 wt%) were sprayed on the cleaned N80 tubing steel substrates, which were subsequently dried at 55 °C for 15 hours. The thickness of the coatings was approximately 300 μm.

### 2.2. Characterization of RGO and RGO-modified EP coatings

The morphology and microstructure of the RGO was investigated via FTIR (WQF-520, Beijing, China) and transmission electron microscopy (TEM, Tecnai G2 F20). The fracture surfaces of RGO-modified EP coatings after liquid nitrogen embrittlement were characterized via SEM (Inspect F50, FEI).

### 2.3. Electrochemical anti-corrosion test

Potentiodynamic polarization curves were plotted and electrochemical impedance spectroscopy (EIS) was conducted to evaluate the corrosion performance of coatings via potentiostat/galvanostat/ZRA (CS-350H, Wuhan Corrtest Instruments Co. Ltd., China). The frequency range was  $10^5$  Hz to  $10^{-2}$  Hz, and the signal was a 10 mV sinusoidal wave. Tafel analysis was conducted to measure the corrosion rates in the range of -0.25 V to 0.25 V (vs. OCP), and the scanning rate was 1 mV/s. A three-electrode system was adopted: a platinum electrode was used as the counter electrode, a saturated calomel electrode (SCE) was used as the reference electrode, and an N80 steel substrate with a coating was used as the working electrode. The working electrode was immersed in 10.0 wt% NaCl solution at 50°C. The impedance and polarization curves of the coatings were measured after 60 days of immersion. Then, Tafel fitting of the potentiodynamic polarization curves and equivalent electrical circuit (EEC) fitting of the EIS results were conducted using the ZSimpWin software.

## 3. RESULTS AND DISCUSSION

### 3.1. Characterization of RGO

FTIR spectra of GO and RGO are presented in Fig. 1. The characteristic absorption bands of GO and RGO at 3447, 1741, 1625, 1200 and 1120  $\text{cm}^{-1}$  correspond to -OH, C=O, C=C, C-O and C-O-O, respectively. For GO, many oxygen groups are distributed on the surface, and the carboxyl and carbonyl groups are distributed on the edges of the sheets [33]. In contrast to the groups of GO, the C=O, C-O

and C-O-O groups in RGO almost disappeared. Therefore, the RGO that is used in this study has a high degree of graphitization.

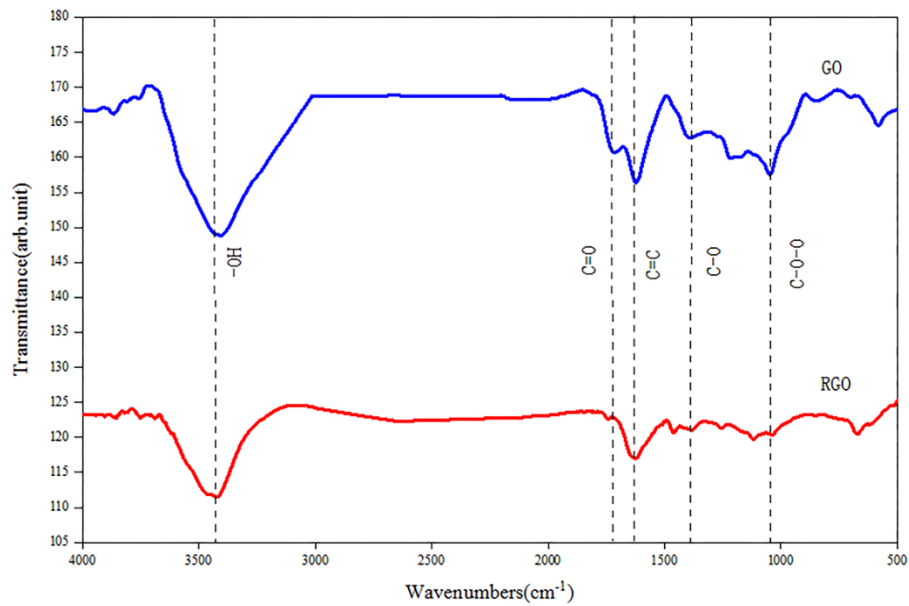


**Figure 1.** FTIR spectra for GO and RGO

The surface morphologies of RGO were identified via TEM. Fig. 2 presents a TEM image of dispersed RGO. The color of the RGO sheets is lighter; hence, the dispersion is satisfactory and there are no large aggregates. Due to the large surface energy of a single layer or several layers of RGO, curling and folding occur at the edges of the RGO sheet [34]. The thermodynamic stability of the two-dimensional structure is maintained by this curling and folding, which results in unique structural characteristics.

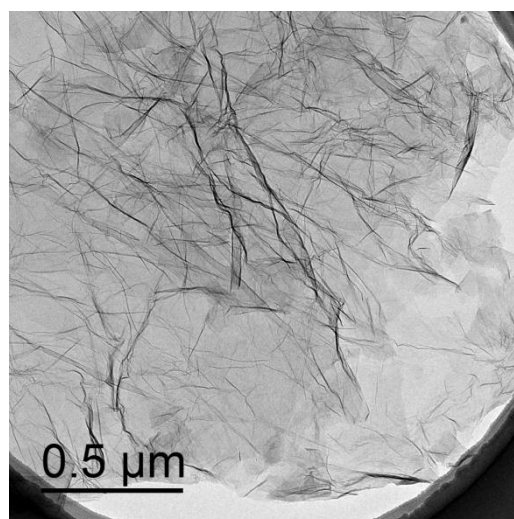


**Figure 2.** TEM photograph of RGO

### 3.1. Characterization of RGO-modified EP coatings

In our previous work, we found that the addition of 1.0 wt% RGO nanosheets effectively reduced the numbers and sizes of the pores in the as-prepared EP composite coatings. To define the variation rules of the sizes of the pores in the EP composite coatings after long-term service, brittle fracture experiments of coatings with various RGO contents were conducted after immersing them at 50°C in 10.0 wt% NaCl solution for 60 days. The fracture surfaces of 0 wt%, 0.5 wt%, 1.0 wt%, 2.5 wt%, and 4.0 wt% RGO-modified EP coatings are shown in Fig. 3. The cross-sectional surface of the 0 wt% RGO-modified EP coating shows a clean fracture surface, thereby implying a brittle fracture. However, in the ductile fracture morphology in Fig. 3(b-e), tearing ridges can be readily observed from the RGO-modified EP coatings, which show RGO that is warped without peeling off the resin matrix. Hence, the interfacial adhesion between the RGO and the EP was strong, and RGO can improve the strength and toughness of EP coatings. In the process of deformation, RGO, which is the stress concentration center, can cause the resin matrix around it to yield and absorb a substantial amount of energy. The interface between RGO and the EP is separated to form holes, which can passivate the cracks and prevent the generation of destructive cracks. Moreover, the specific surface area of RGO is large, which increases the contact area with the EP. If the material is under external force, it can produce more microcracks and absorb a substantial amount of stress. However, as the RGO content was increased to 4.0 wt%, the tearing ridge decreased significantly, which was likely due to the aggregation of the RGO nanosheets.

The pore sizes of the samples were randomly measured, and the top five sizes of pores for each sample are listed in Tab. 1. According to Tab.1, the maximum pore size that was measured on the EP coatings with 0 wt% is 1305 nm, with an average size of 826.5 nm. The addition of 0.5 wt% RGO caused no significant change in the quantity or size of the pores (Fig. 3a and Fig. 3b). However, when the RGO content was 1.0 wt%, the size of the pores decreased by two to three times and the quantity of the pores decreased by two orders of magnitude in the coatings compared to the neat EP coatings (Fig.3c). When the RGO contents were increased to 2.5 wt% and 4.0 wt%, the quantity and size of the pores increased substantially, and the average size of the pores in these coatings even exceeds that in the neat EP coating.

If the coating is subjected to external stress, large pore defects will lead to poor stress transfer and stress concentration, and corrosive media such as H<sub>2</sub>O, O<sub>2</sub> and Cl<sup>-</sup> will enter the coating more easily through the defects and reach the metal substrate surface, thereby forming severe corrosion, which will eventually cause the coating to fall off easily. Many studies have shown that the number of pores in the coating can be decreased by adding graphene into the EP. For example, nano oxide can be used to modify GO and blend with EP to form composite materials, which can fill pores in the coating [35-38]. Zhang [39] prepared a GO-modified EP coating, in which the GO modification effectively reduced the porosity of the coating. However, these studies use graphene to fill the pores, to decrease the number of pores, and the mechanism of graphene in the process of bubble generation is not discussed.

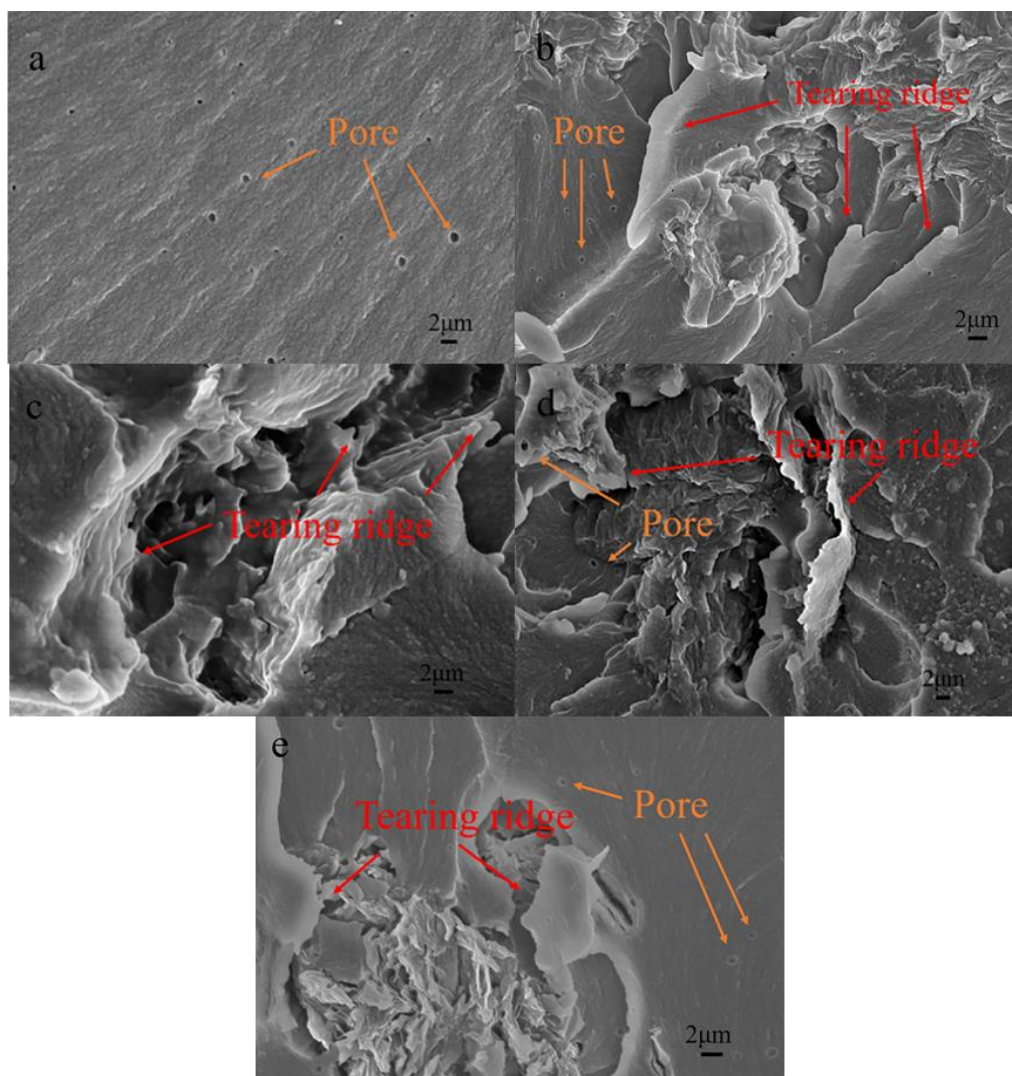


**Figure 3.** SEM images of fractures in the EP coatings with (a) 0 wt%, (b) 0.5 wt%, (c) 1.0 wt%, (d) 2.5 wt%, and (e) 4.0 wt% RGO

In this study, a possible mechanism is proposed: When RGO is dispersed by ultrasonic waves, the high temperature and high pressure of the generated bubbles through the cavitation of the rupture process promotes the uniform dispersion of RGO in EP coatings. Therefore, when the content of RGO is 0.5 wt%, many pores remain in the coatings. As the content of RGO increases, RGO will destroy large bubbles, thereby resulting in small bubbles. This facilitates bubble overflow; hence, the number of pores in the coatings will decrease. However, when the RGO content was increased to 2.5 wt% and 4.0 wt%, aggregation of the RGO nanosheets occurred, which significantly lowered the bubble-breaking effect, thereby resulting in the formation of pores of increased quantity and size in the coatings. Therefore, there is a balance between the pore reduction that is induced by the bubble-breaking effect of RGO nanosheets and the pores increase that is induced by the aggregation of the RGO nanosheets. This balance is realized when the optimal amount of RGO has been added into the coatings. The bubble-breaking effect and the mechanism of RGO will be investigated in our future work. Therefore, the addition of a suitable amount of RGO not only increases the toughness but also decreases the quantity and size of the pores of these coatings in high-temperature and high-salinity environments.

**Table 1.** Pore size on the cross-sectional surfaces of coatings with various RGO contents

Content of RGO	Pore size (nm)					Average size (nm)
0 wt%	435.0	870.0	652.5	870.0	1305.0	826.5
0.5 wt%	431.0	431.0	862.0	1293.0	1115.0	826.4
1.0 wt%	652.5	261.0	211.0	196.0	356.0	335.3
2.5 wt%	862.0	1115.0	1115.0	1293.0	1293.0	1135.6
4.0 wt%	431.0	862.0	1293.0	1293.0	1293.0	1034.4

### 3.3 EIS analysis of RGO-modified EP coatings

EIS and potentiodynamic polarization curves were used to evaluate the corrosion performances of EP coatings with various contents of RGO. Many electrochemical studies on the coating have been conducted by immersing the coatings in 3.5% NaCl solution at room temperature in accordance with the marine simulation environment [23]. For example, GO was introduced into a polypyrrole (PPY) matrix, and PPY-GO composite coatings with various GO contents were electrodeposited in situ on 304 stainless steel (SS) bipolar plates to protect them from corrosion in an aggressive working environment [40]. N. N. Taheri [27] grafted GO particles onto zinc doped polyaniline (PANI), added it to the EP, and immersed it in 3.5% NaCl solution for electrochemical testing. To more closely approximate the conditions of the underground environment of onshore oil wells, prior to the test, the coatings were immersed in 10.0 wt% NaCl solution at 50°C for 60 days, and the results are presented in Fig. 4. The higher the impedance in the Nyquist plot, the better the anti-corrosion effect of the coatings. The addition of RGO increases the radius of the capacitance; hence, the addition of RGO effectively enhances the anticorrosion performance of the EP coating. The effect depends on the chemical stability of RGO. When RGO is added to the EP coating, a retardant layer can be formed, which prevents direct contact between the corrosive media and the substrate, and increases the tortuosity of the diffusion path. Moreover, the RGO is a nanometer-scale material, which can be used to fill the curing defects of the EP coating. Moreover, it is hydrophobic; hence, it can delay the pervasion of water and the corrosion. The TEM image in Section 3.1 shows that there are many folds on the surface of RGO. When it is added to EP as a filler, the folds on the surface can have a larger contact area with the EP, thereby making the diffusion path of active media more tortuous and, thus, substantially improving the corrosion resistance of the coating. Therefore, according to the Nyquist plots and Bode diagrams in Fig. 4, with the increase of the RGO content, the radius of capacitance initially increases and subsequently decreases. The modified EP coating with 1.0 wt% RGO shows excellent corrosion resistance, which is due to its high impedance and large radius of capacitance. However, when the content of RGO is high, agglomeration occurs in the coating, thereby resulting in many defects, such as pores in the EP coating, which provide channels for the diffusion of corrosive media; thus, the anti-corrosion performance of the coating is decreased.

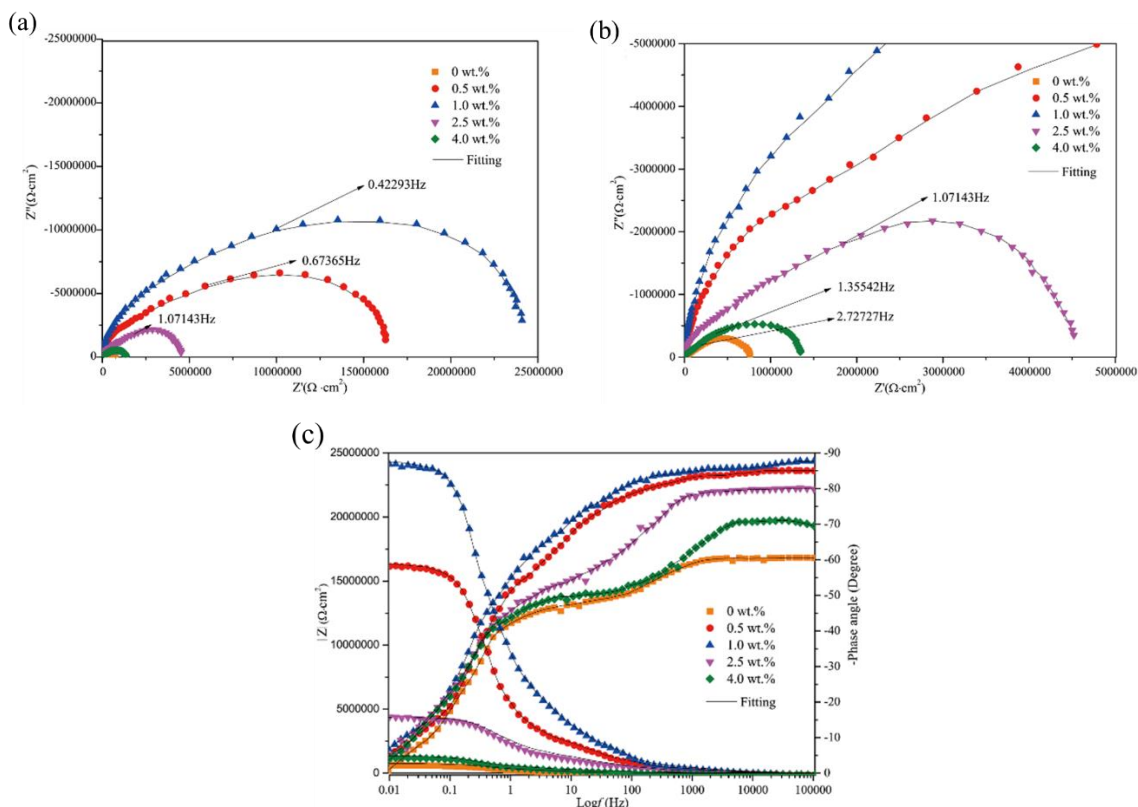


**Figure 4.** (a) Nyquist plots, (b) locally enlarged Nyquist plots, and (c) Bode diagrams of the EP composite coatings after immersion in 10.0 wt% NaCl solution at 50°C for 60 days

To further characterize the anti-corrosion effect of the coatings, the impedance data are analyzed and fitted with the ZSimpWin simulation software. The equivalent circuit and the analysis results are presented in Fig. 5 and Tab. 2. The electronic components  $R_s$ ,  $C_c$ ,  $R_c$ ,  $R_{ct}$  and  $CPE_{dl}$  in the equivalent circuit represent the electrolyte resistance, coating capacitance, coating resistance, charge transfer resistance and double layer capacitance, respectively.  $C_c$  represents the amount of corrosive media that penetrate into the coating,  $R_c$  can be used to represent the number and area of the pores on the coating surface,  $CPE_{dl}$  represents the failure area of the coating, and  $R_{ct}$  represents the resistance value of the charge transfer on the metal surface, which can directly reflect the corrosion rate of the interface between the coating and N80 steel.

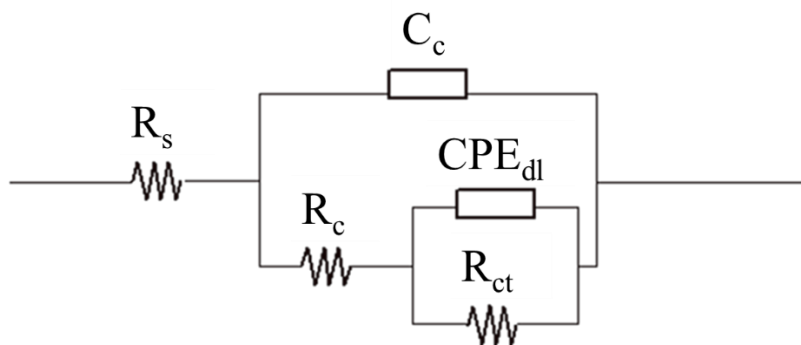


**Figure 5.** Equivalent circuit of the sample

**Table 2.** EIS analysis of electrochemical parameters of the coating samples after immersion in 10.0 wt% NaCl solution for 60 days

Content of RGO	0 wt%	0.5 wt%	1.0 wt%	2.5 wt%	4.0 wt%
$R_{ct} \times 10^6 \Omega \cdot \text{cm}^2$	0.11	2.81	10.16	1.02	0.18
$C_c \times 10^{-10} \text{F} \cdot \text{cm}^{-2}$	314.50	12.31	1.13	15.17	17.48
$R_c \times 10^5 \Omega \cdot \text{cm}^2$	1.11	28.09	101.60	10.18	1.79
$\text{CPE}_{dl} \times 10^{-9} \text{F} \cdot \text{cm}^{-2}$	2.64	21290.00	1.67	36.87	77.35

As summarized above,  $R_c$  ( $1.016 \times 10^7 \Omega \cdot \text{cm}^2$ ) and  $R_{ct}$  ( $1.016 \times 10^7 \Omega \cdot \text{cm}^2$ ) attained their maximum values and  $C_c$  ( $1.127 \times 10^{-10} \text{F} \cdot \text{cm}^{-2}$ ) and  $\text{CPE}_{dl}$  ( $1.67 \times 10^{-9} \text{F} \cdot \text{cm}^{-2}$ ) reached their minimum values when the RGO content was up to 1.0 wt% in the modified EP coatings. Therefore, the optimal addition of RGO is 1.0 wt%. The addition of a suitable amount of RGO can effectively improve the corrosion resistance of EP coatings. However, with the increase of the amount of added RGO, the severity of the defects in the coating increase due to agglomeration. Finally, the corrosion resistance of the coating is decreased.

#### 2.4 Tafel analysis of RGO-modified EP coatings

The potentiodynamic polarization curves are plotted in Fig. 6, and Tab. 3 lists the kinetic parameters that were calculated from the potentiodynamic polarization curves, which include  $I_{\text{corr}}$  and  $E_{\text{corr}}$ . The corrosion current ( $I_{\text{corr}}$ ) decreased significantly and the corrosion potential ( $E_{\text{corr}}$ ) exhibited a positive shift when graphene was added.  $I_{\text{corr}}$  initially decreased and subsequently increased with the increase of the RGO content, while  $E_{\text{corr}}$  initially exhibited a positive shift and subsequently exhibited a negative shift.

This is due to the small-size effect of RGO filling in the pores of the coating. The corrosive media can not penetrate the pore paths that are blocked by RGO t via natural convection mass transfer to the reaction area of the electrode interface corrosion. Due to the consumption of depolarization, the concentrations of  $\text{H}_2\text{O}$ ,  $\text{O}_2$  and  $\text{Cl}^-$  at the bottom of the pores can not be supplemented timely, thereby resulting in a concentration difference with the corrosive media in the solution of the coating surface at the top of the pore. Instead, Faradaic processes of the electrode reaction are controlled by the tangent diffusion of the corrosive media. The electrochemical polarization of the corrosion system is gradually weakened, and concentration polarization occurs.

Compared with neat EP coatings, the corrosion resistance of the coatings with RGO is substantially improved. The modified EP coatings with 1.0 wt% RGO had the lowest corrosion current density ( $9.5172 \times 10^{-9} \text{A}/\text{cm}^2$ ), the highest corrosion potential ( $-0.15107 \text{V}$ ), and the maximum polarization resistance ( $6.04 \times 10^9 \Omega \cdot \text{cm}^2$ ). Therefore, the optimal addition of RGO is 1.0 wt%, which is in accordance with the results of EIS.

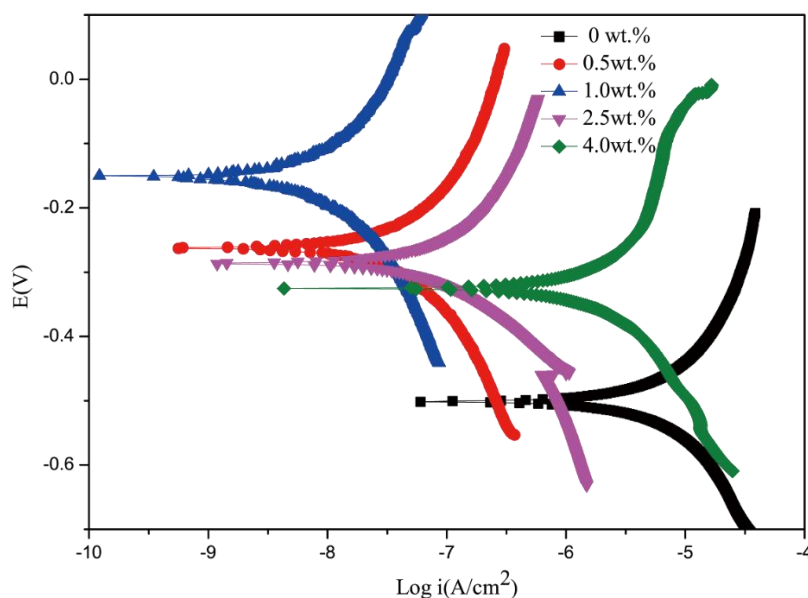


**Figure 6.** Potentiodynamic polarization curves of the EP composite coatings after immersion in 10.0 wt% NaCl solution at 50°C for 60 days

**Table 3.** Electrochemical parameters that were obtained from potentiodynamic polarization curves via Tafel extrapolation for the coated samples after immersion in 10.0 wt% NaCl solution for 60 days

Content of RGO	0 wt%	0.5 wt%	1.0 wt%	2.5 wt%	4.0 wt%
$I_{\text{corr}}$ ( $\mu\text{A}/\text{cm}^2$ )	9.190	0.074	0.009	0.705	5.415
$E_{\text{corr}}$ (V)	-0.501	-0.262	-0.151	-0.287	-0.325

### 3.5 Anti-corrosion mechanism

In this study, after immersion in 10.0 wt% NaCl solution for 60 days, the modified EP coatings with 1.0 wt% RGO still showed superior corrosion resistance to that of the neat EP coatings. Researchers proposed possible anti-corrosion mechanisms of graphene-modified coatings: (1) graphene can decrease the coating porosity [30-32]; (2) graphene causes a barrier effect [30-32]; and (3) graphene can block the cathodic reaction between the coating and the metal interface [41]. As described in the above investigation, the addition of 1.0 wt% RGO nanosheets not only improved the strength and toughness of the coatings but also effectively decreased the size of the pores by two to three times and decreased the quantity of the pores by two orders of magnitude in the coatings compared to neat EP coatings. Therefore, the added RGO nanosheets effectively block the penetration of the corrosive media via the penetration effect and decrease the quantity and size of the pores in the coatings, which results in excellent anticorrosion performance. However, with the increase of the RGO content, RGO nanosheets will agglomerate, the balance between the pores reduction induced by the bubble-breaking effect of the RGO nanosheets and the pore increase that is induced by the aggregation of the RGO nanosheets will be broken, which will increase the severity of the defects in the EP coatings and decrease the corrosion resistance of the coatings.

#### 4. CONCLUSIONS

(1) After immersion in 10.0 wt% NaCl solution at 50°C for 60 days, the EP composite coatings with 1.0 wt% RGO nanosheets still showed improved strength and toughness, with pores that were two to three times smaller and two orders of magnitude less numerous compared to the neat EP coatings.

(2) The modified EP coatings with 1.0 wt% RGO showed excellent corrosion resistance with the lowest corrosion current density ( $9.5172 \times 10^{-9}$  A/cm<sup>2</sup>), the highest corrosion potential (-0.15107 V) and the maximum polarization resistance ( $6.04 \times 10^9$  Ω•cm<sup>2</sup>) after immersion in the 10.0 wt% NaCl solution for 60 days at 50°C.

#### ACKNOWLEDGEMENTS

This work was supported by the National Natural Science Foundation of China (NO. 51804335): Corrosion resistance and mechanism of graphene-modified epoxy coatings in a coupled oil and water multi-phase medium; Major science and technology projects of Petro China Co. Ltd. (2018E-11-06): Key technologies for improving the development level in complex fault block oilfields at the high water cut stage; and The National Key Research and Development Program of China (2019YFF0217504): Research and application of common technologies in the national quality foundation-The complete process inspection and quality control technology of 13Cr / 110SS products in service.

#### References

1. X. M. Shi, T. A. Nguyen, Z. Y. Suo, Y. J. Liu and R. Avci, *Surface and Coatings Technology*, 204 (2009) 237.
2. I. Zaman, T. T. Phan, H. C. Kuan, Q. S. Meng, L. T. B. La, L. Luong, O. Youssf and J. Ma, *Polymer*, 52 (2011) 1603.
3. S. Chatterjee, J. W. Wang, W. S. Kuo and N. H. Tai, *Chemical Physics Letters*, 531 (2012) 6.
4. J. P. Pascault, R. J. J. Williams, *Polymer Bulletin*, 24 (1990) 115.
5. D. Chmielewska, T. Sterzyński, and B. Dudziec, *Journal of Applied Polymer Science*, 131 (2014) 8444.
6. S. Hichem, E. M. M. Lassaad, H. Guerhazi, S. Agnel and A. Toureille, *Journal of Alloys and Compounds*, 477 (2009) 316.
7. Y. G. Liu, *Corrosion & Protection*, 8 (2003) 361 (In Chinese).
8. Y. Y. Ge, C. J. Han, Y. Q. Yuan, X. Y. Ma, S. F. Sheng and Y. C. Deng, *Henan Petroleum*, 19 (2005) 76 (In Chinese).
9. G. P. He, Q. Y. Yang, *Journal of Jiangnan Petroleum University of Staff and Workers*, 22 (2009) 56 (In Chinese).
10. J. Z. Li, *Inner Mongolia Petrochemical Industry*, 20 (2013) 41 (In Chinese).
11. A. Bisht, K. Dasgupta, and D. Lahiri, *Journal of Applied Polymer Science*, 135 (2018) 46101.
12. A. Montazeri, J. Javadpour, A. Khavandi, A. Tcharkhtchi and A. Mohajeri, *Materials & Design*, 31 (2010) 4202.
13. S. Chhetri, N. C. Adak, P. Samanta, P. K. Mallisetty, N. C. Murmu and T. Kuila, *Journal of Applied Polymer Science*, 135 (2018) 46124.
14. H. Feng, X. D. Wang, and D. Z. Wu, *Industrial & Engineering Chemistry Research*, 52 (2013) 10160.
15. R. J. Day, P. A. Lovell, and A. A. Wazzan, *Composites Science and Technology*, 61 (2001) 41.
16. R. Bagheri, R. A. Pearson, *Polymer*, 41 (2000) 269.
17. T. Kawaguchi, R. A. Pearson, *Polymer*, 15 (2003) 4239.

18. S. H. Lee, D. R. Dreyer, J. An, A. Velamakanni, R. D. Piner, S.J. Park, Y.W. Zhu, S. O. Kim, C. W. Bielawski and R. S. Ruoff, *Macromolecular Rapid Communications*, 31 (2010) 281.
19. G. X. Wang, X. P. Shen, B. Wang, J. Yao and J. Park, *Carbon*, 47 (2009) 1359.
20. Q. F. Jing, W. S. Liu, Y. Z. Pan, V. V. Silberschmidt, L. Li and Z. L. Dong, *Materials & Design*, 85 (2015) 808.
21. T. Kuilla, S. Bhadra, D. H. Yao, N. H. Kim, S. Bose and J. H. Lee, *Progress in Polymer Science*, 35 (2010) 1350.
22. M. Naderi, M. Hoseinabadi, M. Najafi, S. Motahari and M. Shokri, *Journal of Applied Polymer Science*, 135 (2018) 46201.
23. H. H. Di, Z. X. Yu, Y. Ma, Y. Pan, H. Shi, L. Lv, F. Li, C. Wang, T. Long and Y. He, *Polymers Advanced Technologies*, 27 (2016) 915.
24. Y. H. Tang, D. Xiang, D. H. Li, L. Wang, P. Wang and P. D. Han, *Surface Technology*, 47 (2018) 203.
25. J. A. Q. Rentería, L. F. C. Ruiz, and J. R. R. Mendez, *Carbon*, 122 (2017) 266.
26. Y. H. Wu, X. Y. Zhu, W. J. Zhao, Y. J. Wang, C. T. Wang and Q. J. Xue, *Journal of Alloys and Compounds*, 777 (2019) 135.
27. N. N. Taheri, B. Ramezanzadeh, and M. Mahdavian, *Journal of Alloys and Compounds*, 800 (2019) 532.
28. M. S. Selim, S. A. El-Saftya, N. A. Fatthallahd and M. A. Shenashen, *Progress in Organic Coatings*, 121 (2018) 160.
29. F. D. Meng, T. Zhang, L. Liu, Y. Cui and F. H. Wang, *Surface and Coatings Technology*, 361 (2019) 188.
30. C. Feng, L. J. Zhu, Y.Q. Cao, Y. Di, Z.X. Yu and G. H. Gao, *International Journal of Electrochemical Science*, 14 (2019) 1855.
31. C. Feng, L. J. Zhu, Y. Q. Cao, Y. Di, Z. X. Yu and G.H. Gao, *International Journal of Electrochemical Science*, 13 (2018) 8827.
32. L. J. Zhu, C. Feng, and Y. Q. Cao, *Applied Surface Science*, 493 (2019) 889.
33. A. Dimiev, D. V. Kosynkin, L. B. Alemany, P. Chaguine and J. M. Tour, *Journal of the American Chemical Society*, 134 (2012) 2815.
34. D. R. Nelson, T. Piran, and S. Weinberg, *World Scientific*, 2004, Singapore.
35. Z. X. Yu, H. H. Di, Y. Ma, Y. He, L. Liang, L. Lv, X. Ran, Y. Pan and Z. Luo, *Surface and Coatings Technology*, 276 (2015) 471.
36. Z. X. Yu, H. H. Di, Y. Ma, L. Lv, Y. Pan, C. L. Zhang, Y. He, *Applied surface science*, 351 (2015) 986.
37. Y. Ma, H. H. Di, Z. X. Yu, L. Liang, L. Lv, Y. Pan, Y. Y. Zhang and D. Yin, *Applied surface science*, 360 (2016) 936.
38. H. H. Di, Z. X. Yu, Y. Ma, F. Li, L. Lv, Y. Pan, Y. Lin, Y. Liu and Y. He, *Journal of the Taiwan Institute of Chemical Engineers*, 64 (2016) 244.
39. Z. Y. Zhang, W. H. Zhang, D. S. Li, Y. Y. Sun, Z. Wang, C. L. Hou, L. Chen, Y. Cao and Y. Q. Liu, *International journal of molecular sciences*, 16 (2015) 2239.
40. L. Jiang, J. A. Syed, H. B. Lu and X. K. Meng, *Journal of Alloys and Compounds*, 770 (2019) 35.
41. S. S. Chen, L. Brown, M. Levendorf, W. W. Ca, S. Y. Ju, J. Edgeworth, X. S. Li, C. W. Magnuson, A. Velamakanni, R. D. Piner, J. Y. Kang, J. Park and R. S. Ruoff, *ACS Nano*, 5 (2011) 1321.